Astron. Astrophys. 336, 200–208 (1998)

ASTRONOMY AND ASTROPHYSICS

ASCA observation of the polar RX J1802.1+1804

M. Ishida[1], **J. Greiner**[2⋆], **R.A. Remillard**[3], **and C. Motch**[4]

[1] Institute of Space and Astronautical Science, 3-1-1 Yoshinodai, Sagamihara, Kanagawa 229, Japan (ishida@astro.isas.ac.jp)
[2] Max-Planck-Institut für Extraterrestrische Physik, D-85740 Garching, Germany
[3] Center for Space Research, MIT, 77 Mass Ave, Cambridge, MA 02139, USA (rr@space.mit.edu)
[4] Observatoire de Strasbourg, 11 rue de l'Université, F-67000 Strasbourg, France (motch@astro.u-strasbg.fr)

Received 22 December 1997 / Accepted 14 April 1998

Abstract. We present X-ray data of RX J1802.1+1804 obtained by *ASCA*. Although it shows a clear orbital intensity modulation with an amplitude of nearly 100% below 0.5 keV in *ROSAT* data, the *ASCA* light curves are nearly flat except for a possible dip lasting about one-tenth of the orbital period. We discuss this within the model assumption of a stream-eclipsing geometry as derived from the ROSAT observations.

The *ASCA* X-ray spectrum can be represented by a two temperature optically thin thermal plasma emission model with temperatures of $\sim$1 keV and $>$7 keV, suggesting postshock cooling as observed in EX Hya. A remarkable feature of the spectrum is the strong iron $K\alpha$ emission line whose equivalent width is $\sim$4 keV. To account for this, an iron abundance of greater than at least 1.3 times Solar is required. A combined spectral analysis of the *ROSAT* PSPC and *ASCA* data indicates that the $N_{\rm H}$-corrected flux ratio of the soft blackbody (0.1–2.4 keV) to the hard optically thin thermal plasma emission (2–10 keV) is as large as $\sim 10^4$.

Key words: stars: novae, cataclysmic variables – accretion, accretion disks – X-rays: stars – stars: individual: RX J1802.1+1804 = V884 Her

1. Introduction

A polar (or AM Her type object; Cropper 1990) is an accreting binary composed of a mass-donating low mass secondary star and a magnetized white dwarf with a field strength of the order of 10-100 MG. Matter from the secondary accretes along the field lines onto a small region of the white dwarf close to the magnetic pole. Since the flow is highly supersonic, a standing shock is formed close to the white dwarf, and a hot plasma with a temperature of 10^8 K is formed. From the postshock plasma, optical cyclotron emission and optically thin thermal plasma emission in X-rays have been observed. In addition to this, blackbody emission with a temperature of 10–40 eV is observed. Although the blackbody component is considered to be radiated from the surface of the white dwarf around the postshock plasma via reprocessing of the cyclotron and the hard X-ray radiation, its intensity is usually much larger than that of the cyclotron and hard X-ray radiation. This has become known as the so-called 'soft excess problem' (Rothschild et al. 1981). Beuermann and Burwitz (1995) recently suggested that the amount of the soft excess is correlated with the strength of the magnetic field of the white dwarf.

It is known that the hard X-ray continuum spectrum of magnetic cataclysmic variables (mCVs) can, to a first approximation, be fitted by an optically thin thermal plasma emission spectrum with a single temperature undergoing photoelectric absorption represented by a single hydrogen column density. To represent the *EXOSAT* spectra of intermediate polars, Norton and Watson (1989) introduced the so-called 'partial-covering absorber model' in which photoelectric absorption was represented by two column densities. Complex absorption was found also in polars with *Ginga* observations (Ishida and Fujimoto 1995).

It has also been expected that the hard X-ray emitting hot plasma is gradually cooled by cyclotron emission and bremsstrahlung (Aizu 1973, Frank, King and Lasota 1983, Imamura and Durisen 1983), and that the hard X-ray spectrum consists of multi-temperature emission components. Such a multi-temperature emission spectrum was first suggested by an *Einstein* observation of EX Hya (Singh & Swank 1993), and later was established by an *ASCA* observation (Ishida, Mukai and Osborne 1994, Fujimoto and Ishida 1997). Note, however, that it is only for EX Hya that the existence of multi-temperature emission is confirmed observationally.

RX J1802.1+1804 was discovered during the search for supersoft X-ray sources in the *ROSAT* all-sky survey data (Greiner, Remillard and Motch 1995). Greiner, Remillard and Motch (1995, 1998) have analyzed all the *ROSAT* data taken between 1990 September and 1993 September, and found a coherent period of 0.07847977(11) d (= 1.8835145$\pm$0.000003 hr). The pulse profile in the band < 0.5 keV is characterized by a deep intensity minimum, with basically no X-ray flux, lasting 0.1 orbital phase. The X-ray spectrum is characterized by strong blackbody emission with a temperature of 20 ± 15 eV, with a clear excess emission above 1 keV, which has been

Send offprint requests to: M. Ishida

⋆ Present address: Astrophysical Institute Potsdam, An der Sternwarte 16, D-14482 Potsdam, Germany (jgreiner@aip.de)

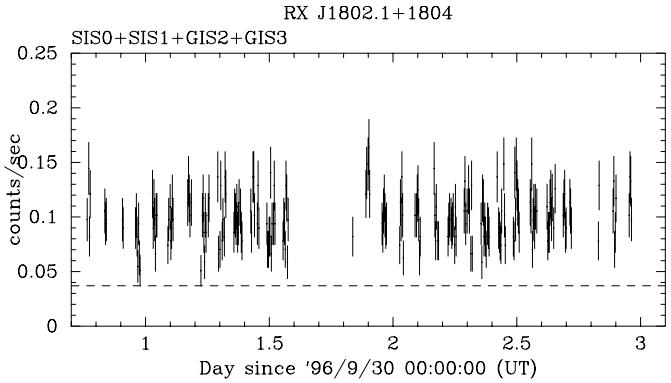

Fig. 1. Light curve of RX J1802.1+1804 from all the four detectors in the band 0.5–10 keV with 256 sec binning. The horizontal dashed line indicates the background level.

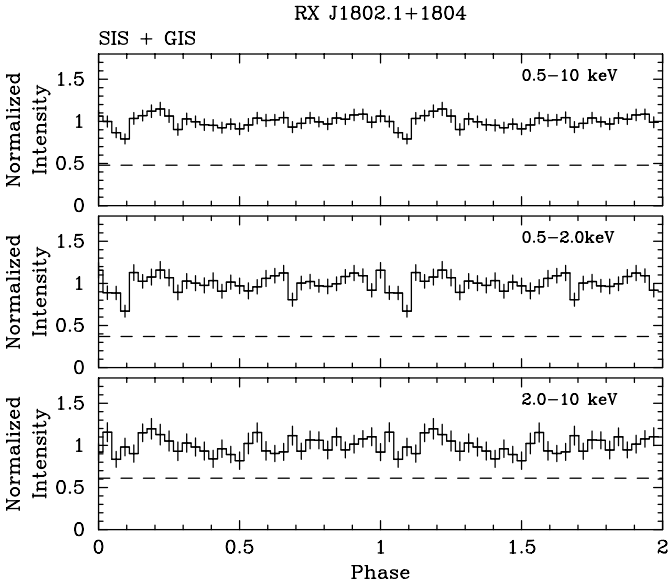

Fig. 2. Energy-resolved light curves of RX J1802.1+1804 folded with the *ROSAT* ephemeris (Eq. (1), Greiner, Remillard and Motch 1995, 1998). The energy bands of the light curves are shown at the upper right corner of each panel. Dashed lines indicate the background level in each panel.

approximated by thermal bremsstrahlung with a temperature of 20 keV. The absorption-corrected 0.1–2.4 keV fluxes of the blackbody and the thermal bremsstrahlung components are 7×10^{-11} erg cm^{-2}s^{-1} and 8×10^{-13} erg cm^{-2}s^{-1}, respectively, suggesting a huge soft excess of nearly 90 in the 0.1–2.4 keV band. Szkody et al. (1995) carried out photometry, spectroscopy and polarimetry in the optical band, and found several characteristics of polars such as HeII emission line stronger than Hβ and circular polarization of 4%. All these properties strongly indicate that RX J1802.1+1804 is a polar.

In this paper, *ASCA* data of RX J1802.1+1804 taken in 1996 Sep-Oct are presented. In Sect. 2 we describe how the *ASCA* observation was carried out. In Sect. 3 light curve and spectral analysis are presented. We discuss these properties in Sect. 4 in combination with the *ROSAT* and *IUE* data. In Sect. 5 we summarize our results.

2. Observation

The *ASCA* observation of RX J1802.1+1804 was carried out between 1996 September 30.75 and October 2.96 (UT). *ASCA* is equipped with four equivalent X-ray Telescopes (XRT: Serlemitsos et al. 1995). In the common focal plane, two Solid-state Imaging Spectrometers (SIS: Burke et al. 1994, Yamashita et al. 1997) and two Gas Imaging Spectrometers (GIS: Makishima et al. 1996, Ohashi et al. 1996) are mounted. The SIS has high sensitivity in the lower energy bandpass and high energy resolution of $\Delta E/E \simeq 0.02$ (at the time of launch), whereas the GIS has high throughput in the higher energy bandpass and high time resolution.

Throughout the observation, the GIS operated in Pulse Height normal mode in which the band 0.7-10 keV is covered by 1024 pulse height channels. The SIS mode was switched between the 1-CCD FAINT mode in high bit rate and the 1-CCD BRIGHT mode in medium bit rate, which cover 0.4-10 keV with 4096 and 2048 pulse height channels, respectively. The observation was performed normally except for loss of data during October 1.57–1.83 (UT) because of a sudden cancelation of the Deep Space Network service.

3. Analysis and results

3.1. Data selection

We have screened the data with the following criteria. The data taken while the spacecraft passes the South Atlantic Anomaly are discarded. In order to avoid the Earth-limb effect, we have only chosen data when the Earth elevation angle of RX J1802.1+1804 exceeds 5°. In addition to this, we have also discarded the SIS data while the elevation angle from the sunny Earth limb is less than 10°. For the SIS, we have skipped day-night transition periods of the spacecraft which occur during every satellite orbit. With these selection criteria, some 77 ksec exposure time is retained for both the SIS and the GIS.

For the integration of the X-ray source photons, we have adopted an aperture of 3′.7 and 4′.0 in radius centered on RX J1802.1+1804 for the SIS and GIS, respectively. For the background, the entire CCD chip outside the aperture is used for the SIS (there are no other X-ray sources within the field of view), whereas an annular region which has the same distance from the boresight of the XRT as the source-integration region is adopted for the GIS.

In Fig. 1, we show the light curve of RX J1802.1+1804 from all the four detectors in the 0.5–10 keV band with 256 sec binning after the data screening as described above. Because *ASCA* is a low-Earth orbit satellite, the source is usually occulted by the Earth every 96 min. (satellite orbital period). As mentioned in Sect. 2, approximately 6 hrs of data are lost in the middle of the observation due to a failure of data retrieval on a ground station. The average background-subtracted counting rate is 0.052 c s^{-1} with all the four detectors (0.035 c s^{-1} for the two SIS, and 0.017 c s^{-1} for the two GIS).

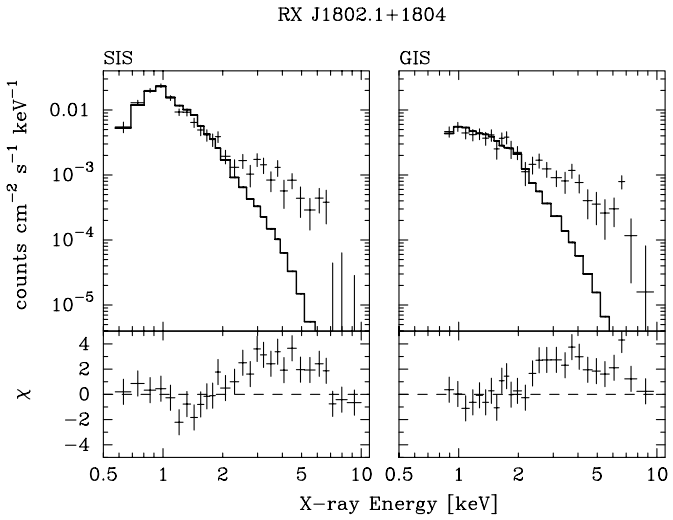

Fig. 3. Combined spectral fit to the SIS and the GIS data with a single Raymond-Smith model.

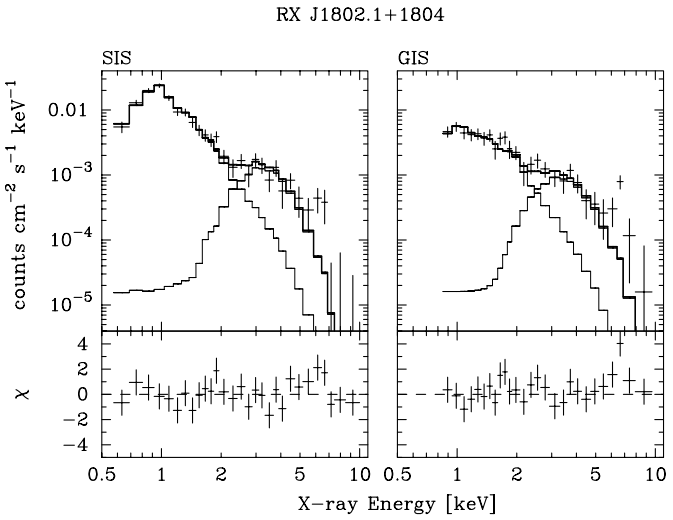

Fig. 4. Combined spectral fit to the SIS and the GIS data with a single Raymond-Smith model undergoing partial covering absorption.

3.2. Energy-resolved light curves

Fig. 2 shows the folded light curves from all the four detectors in the 0.5–10 keV band and in three separate energy bands. In folding the light curves, we have adopted the ephemeris determined from *ROSAT* and optical observations (Greiner, Remillard and Motch 1995, 1998), which is

$$T(HJD) = 2449242.3124(21) + 0.07847977(11) \times E. \quad (1)$$

This ephemeris is accurate enough to predict the time of the dip with an error of only several minutes (phase uncertainty of ± 0.02) at the time of the *ASCA* observation. However, unlike the *ROSAT* light curves which show a modulation amplitude of 100% below 0.5 keV, the *ASCA* light curves are extremely flat except for a possible dip during the phase 1.0–1.1. From the average counting rates of the two phase bins around phase 1.08, we have obtained the depth of the dip to be $33 \pm 14\%$, $35 \pm 23\%$ and $< 54\%$ of the phase-averaged intensity for the bands 0.5–10 keV, 0.5–2 keV and 2–10 keV, respectively, at the 90% confidence level. With the dip duration and depth, it is possible for this dip to correspond to that found in the *ROSAT* light curve, although this is not conclusive. If we assume that the dip seen in Fig. 2 is the same as the one in the *ROSAT* observation, the best-fit period would become slightly longer (0.07848022(16) days) but inconsistent with the ROSAT folding.

3.3. ASCA spectra

Since no remarkable intensity variation is found during the observation, we sum up all the data. According to the data selection criteria described in Sect. 2, we have extracted the source and the background spectra separately for the four detectors. Then we have summed the two SIS spectra and the two GIS spectra, and have created background subtracted SIS and GIS spectra, respectively. Hereafter, we derive spectral parameters of RX J1802.1+1804 by a combined fit of the SIS and GIS spectra using XSPEC version 9.01 (Arnaud 1996).

We have first tried to fit the spectra with a single temperature optically thin thermal plasma model (Raymond and Smith 1977, hereafter referred to as R&S model) undergoing photoelectric absorption. We note that a thermal bremsstrahlung model has conventionally been used to fit X-ray spectra of mCVs. However, optically thin thermal plasma also produces plenty of emission lines from abundant heavy elements. Among them, the iron L-lines appearing between 0.7–2 keV cause a significant excess above the continuum especially in the case that the plasma temperature is lower than $\sim$ 3 keV. It is very difficult to resolve them from the continuum spectrum even with the high spectral resolution of the *ASCA* SIS. In addition, there are a few more processes in the optically thin thermal plasma that produce continuum emission, such as the free-bound transition and the two-photon decay. Under these circumstances, we cannot estimate the continuum parameters if we use the thermal bremsstrahlung model. Hence we will substitute the thermal bremsstrahlung model by a R&S model throughout this paper, except when fitting the spectrum in the band 4–10 keV, because the continuum in this band is always dominated by the thermal bremsstrahlung.

The result of the R&S model fit is shown in Fig. 3, and the best fit parameters are listed in the third column of Table 1. Although the fit seems good below $\sim$2 keV, it obviously shows excess emission above $\sim$2 keV. The most remarkable structure in the residual is the iron emission line appearing in the 6–7 keV band. If we evaluate this with a thermal bremsstrahlung model plus a Gaussian line in the 4–10 keV band, the equivalent width becomes 4.0 ± 1.7 keV. Note that *Ginga* observations indicated that the equivalent width was in the range 0.2–0.8 keV for a dozen of mCVs (Ishida and Fujimoto 1995). Hence the equivalent width of RX J1802.1+1804 is roughly an order of magnitude larger than that of mCVs observed by *Ginga*, indicating a greater abundance by the same order.

Table 1. Spectral parameters of the combined fits to the SIS and the GIS spectra.

Model		1Abs∗1RS	2Abs∗1RS	2Abs∗1RS +GA	1Abs∗2RS	1Abs∗2RS +GA
kT_1	[keV]	~ 0.9	$0.97\,^{1.03}_{0.84}$	$0.94\,^{1.02}_{0.82}$	$0.86\,^{0.89}_{0.82}$	$0.87\,^{0.89}_{0.84}$
kT_2	[keV]	—	—	—	$10.3\,^{18.9}_{6.7}$	$30\,^{\infty}_{7.1}$
Abundance	[Solar]	~ 0.1	$0.14\,^{0.23}_{0.09}$	$0.13\,^{0.21}_{0.08}$	$5.8\,^{16.9}_{2.5}$	$0.82\,^{8.3}_{0.26}$
$N_{\rm H1}$	[10^{21} cm^{-2}]	~ 0.1	< 1.6	<1.9	< 0.6	< 0.8
$N_{\rm H2}$	[10^{21} cm^{-2}]	—	$130\,^{170}_{100}$	$130\,^{170}_{100}$	—	—
Cover. Frac.	[%]	—	$96\,^{97}_{95}$	$97\,^{98}_{96}$	—	—
Line Center	[keV]	—	—	$6.55\,^{6.64}_{6.47}$	—	$6.55\,^{6.67}_{6.36}$
Intensity	[10^{-5} phs s^{-1}cm^{-2}]	—	—	$1.4\,^{1.9}_{1.0}$	—	$0.79\,^{1.16}_{0.42}$
Equiv. Width	[keV]	—	—	$12\,^{15}_{8}$	—	$1.8\,^{2.7}_{1.0}$
χ^2_ν (dof)		3.72(52)	1.21(50)	0.68(48)	0.74(50)	0.69(48)

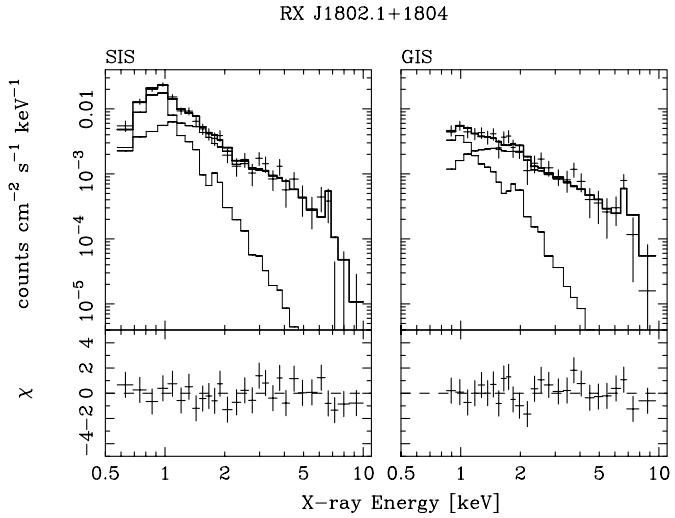

Fig. 5. Combined spectral fit to the SIS and the GIS data with a two temperature Raymond-Smith model.

In order to explain the excess emission above the single component model, we have tried the two possibilities described in Sect. 1, i.e. applying a partial-covering absorption model and introducing a second R&S component.

We first have attempted to apply the partial-covering absorption model to the observed spectra. The result is shown in Fig. 4 and the best fit parameters are summarized in the 4th column of Table 1. The reduced χ^2 value of 1.21 means that despite the improvement over the single R&S model the partial-covering absorption model is only marginally acceptable. The best fit values of the two hydrogen column densities are $< 2 \times 10^{21}$ cm^{-2} and 1.3×10^{23} cm^{-2} and the covering fraction of the latter over the emission region is 97 ± 1%. From *ROSAT* spectra a ratio of soft blackbody flux to hard bremsstrahlung flux of nearly 90 in the 0.1–2.4 keV band was deduced (Greiner, Remillard and Motch 1995, 1998). This extreme soft excess now vanishes because of the high covering fraction of the heavily absorbed component. But the model still does not reproduce the prominent iron emission line which is seen between 6-7 keV. We have thus added a Gaussian, and have fitted the spectra again. The result is summarized in the 5th column of Table 1 and shows that the χ^2 value decreases by nearly 30 after adding two free parameters into the model. Hence, the introduction of the Gaussian is statistically justified. Note, however, that the resulting line equivalent width becomes ~ 12 keV which is unacceptably large. Since the temperature of the emission component is lower than 1 keV, it seems unlikely that this emission line comes from the hot plasma itself. The fluorescent iron emission line is, on the other hand, expected to emanate from the white dwarf surface illuminated by the hard X-ray emission. However, its equivalent width is estimated to be $\sim$ 140 eV (George and Fabian 1991, Done et al. 1994, Beardmore et al. 1995) if the white dwarf surface has solar composition of heavy elements. Therefore, the equivalent width determined from the fit indicates an abundance of the order of $\sim$100 times Solar, which is in strong contradiction to the abundance from the R&S model, ~ 0.1 (Table 1). We conclude that the partial-covering absorption model cannot reproduce the observed spectrum in a physically consistent manner.

As the next step, we have tried to fit the hard excess component shown in Fig. 1 by introducing a second R&S component. The result of the fit is shown in Fig. 5, and the best fit parameters are shown in the 6th column of Table 1. The fit is acceptable with a reduced χ^2 value of 0.74, suggesting that the X-ray spectrum of RX J1802.1+1804 consists of multi-temperature optically thin thermal plasma emission components. The obtained flux is 4.8×10^{-13} erg s^{-1} cm^{-2} in the band 2–10 keV.

Note that this fit still suggests a very high abundance of 6 times Solar with a lower limit of 2.5 times Solar, which seems too high for cataclysmic variables, because they are generally considered to be old systems.

Recently, Hellier et al. (1998) compiled spectra of 15 mCVs from *ASCA* archival data. A total of 14 spectra out of the 15 show a significant fluorescent iron $K\alpha$ emission line at 6.41 keV, as well as the two thermal plasma components at 6.68 keV and 6.97 keV. Among them, the fluorescent component probably originates from the white dwarf surface (Done, Osborne and Beardmore 1995). Although the statistics of our data is not good enough to resolve these three components, it is necessary to include the fluorescent iron $K\alpha$ line into the model in evaluating the abundance correctly.

We thus have introduced a Gaussian line as representing the iron $K\alpha$ line of fluorescence origin. The result is summarized

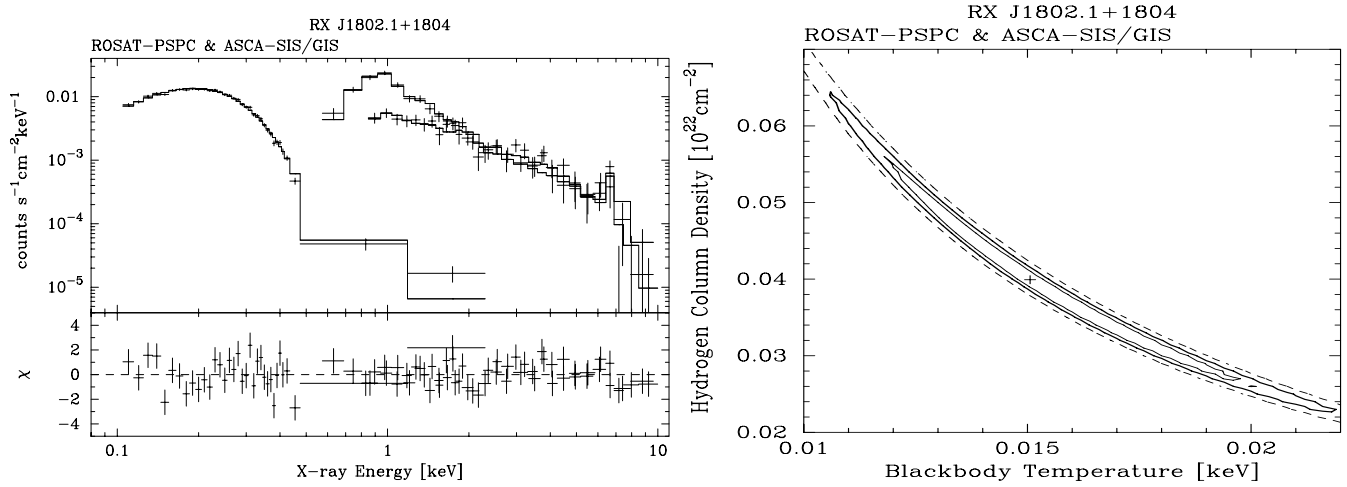

Fig. 6. Combined fit to the *ROSAT* PSPC and the *ASCA* SIS/GIS spectra with a blackbody and a two temperature thin thermal plasma model (left), and the confidence contours of $N_{\rm H}$ vs. kT for the blackbody component. The contours are 68% (innermost), 90% and 99% confidence levels.

in the last column of Table 1. Although the best fit abundance is reduced to ∼0.9, the equivalent width of the fluorescent iron $K\alpha$ line becomes around 2 keV. This value again indicates an abundance of more than 10 times Solar. Clearly, the abundances estimated from the intensities of iron $K\alpha$ lines of the hot plasma origin and of the fluorescence origin should be consistent. This point will be discussed in Sect. 4. Note also that the high abundance can affect the estimation of the bolometric luminosity of the hard component, since the line emission predominates among all the cooling processes in the plasma the temperature of which is less than 2 keV (McCray 1987). We therefore calculate the bolometric luminosity of the hard optically thin thermal component later in relation with the abundance.

3.4. Combined spectral fit of ROSAT and ASCA

Greiner, Remillard and Motch (1995, 1998) reported that the flux of the soft blackbody component is greater than that of the hard thin thermal plasma emission by two orders of magnitude in the band 0.1–2.4 keV. We have attempted to re-examine this extreme soft excess in combination with the *ASCA* hard X-ray data.

ROSAT pointed RX J1802.1+1804 four times between 1992 October and 1993 September. We have extracted a mean *ROSAT* PSPC spectrum from the observation on 1993 September 11/12 (the exposure time of which was ∼ 13 ksec, the longest of all the pointing observations). Details of the observations are presented in Greiner, Remillard and Motch (1998) (see also Greiner, Remillard and Motch 1995).

Since the *ROSAT* observation is not simultaneous with the *ASCA* observation, we have first checked if the intensity levels of the two observations are consistent. To do this, we have used the *ROSAT* PSPC and the *ASCA* SIS and GIS spectral channels below 2 keV, and have fitted a model consisting of a soft blackbody and a hard thin thermal plasma spectrum undergoing photoelectric absorption represented by a common hydrogen column density. Although the temperatures of both components, the normalization of the blackbody as well as the abundance of the thin thermal plasma are constrained to be the same among the three spectra, the normalization of the thin thermal component is set free to vary independently (note that the blackbody parameters are determined solely by the PSPC spectrum). The resulting normalizations of the hard thin thermal emission of the SIS/GIS relative to that of the PSPC are 1.03 and 1.09, respectively, with a typical statistical error of $\sim \pm 0.3$. We thus regard the intensity level of the hard component as the same between the *ROSAT* and the *ASCA* observations.

Next, we have performed a combined spectral fit in the entire 0.1–10 keV band with a model composed of a blackbody and a two temperature thin thermal plasma emission component. The result is shown in Fig. 6.

The fit is marginally acceptable at the 90% confidence level, with χ^2_ν of 1.15 for 83 degrees of freedom. The confidence contours for the hydrogen column density and the temperature of the blackbody component are also shown in Fig. 6. The best fit temperature of the blackbody is obtained to be 15^{+7}_{-5} eV for two parameters of interest. The observed flux of the blackbody is 5.6×10^{-12} erg cm^{-2} s^{-1} in the band 0.1–2.4 keV. After $N_{\rm H}$ correction, the flux becomes 5.1×10^{-9} erg cm^{-2} s^{-1}, which is $\sim 10^4$ times as large as that of the hard component in the 2–10 keV band (Sect. 3.3). The major difference to Greiner, Remillard and Motch (1998) is that the blackbody temperature now is even lower than in the fit of the *ROSAT* data alone, because a part of the emission around ≈0.5 keV is now attributed to the low-kT R&S component.

Because the blackbody temperature is very low, it is very difficult to calculate the bolometric luminosity of the blackbody, because even the *ROSAT* PSPC can observe only the high energy end of the Wien tail. Assuming a disc-shape emission region and a distance of 100 pc, we obtain a bolometric luminosity of the blackbody component $L_{\rm BB}$ of 1.6×10^{34} erg s^{-1}/$< \cos\theta >$ for the best fit temperature of 15 eV, where $< \cos\theta >$ implies the

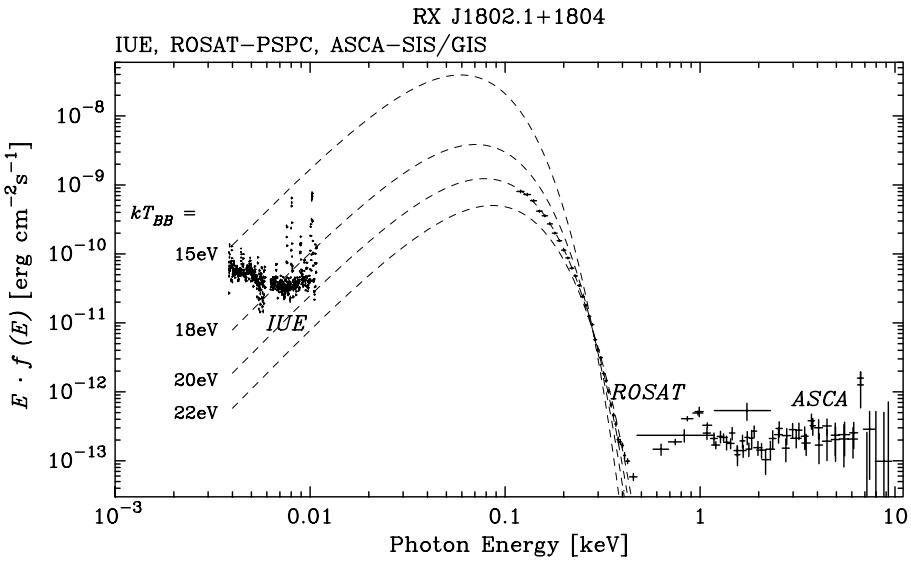

Fig. 7. Intrinsic spectra of *IUE*, *ROSAT* and *ASCA*. $N_{\rm H}$ is corrected for the latter two. The temperature of the blackbody is assumed to be 20 eV for the *ROSAT* spectrum (Sect. 3.4). For the *IUE* spectrum, extinction correction is smaller than a factor 2 and has not been applied. $N_{\rm H}$- corrected blackbody models from the *ROSAT* and *ASCA* combined fitting are also drawn by dashed lines in the temperature range 15–22 eV. The allowed range of the blackbody temperature becomes tightly constrained to 20-22 eV by including the *IUE* data (Shrader et al. 1997).

cosine of the angle between the normal of the disk and the line of sight. However, the 90% confidence range of $L_{\rm BB}$ becomes $2 \times 10^{32} - 1 \times 10^{37}$ erg s^{-1} for the temperature of 22–10 eV.

3.5. Constraint on the soft component from IUE data

To further constrain the spectral parameters of the soft (blackbody) component, we have utilized the *IUE* observation performed on 1995 Aug. 31 (Shrader et al. 1997). Among the several exposures of *IUE*, we collected the data taken out of the X-ray eclipse, which are SWP55775/6 and LWP31382 using the ephemeris of Greiner, Remillard and Motch (1998). For SWP, we took the time average of the two exposures. In Fig. 7, we have plotted the *IUE* spectra thus obtained together with $N_{\rm H}$-corrected spectra of *ROSAT* ($kT = 20$ eV) and *ASCA* in a $\nu F(\nu)$ diagram. Note that we have not corrected the color of the *IUE* spectrum. The correction factor at 1000 Å is, however, less than 2 from the hydrogen column density 3.2×10^{20} cm^{-2} (Greiner, Remillard and Motch 1998), and even smaller at longer wavelengths.

We have also shown the $N_{\rm H}$-corrected best fit blackbody spectra obtained from the simultaneous *ROSAT* and *ASCA* spectral fitting (Sect. 3.4). It is obvious that the shape of the *IUE* spectrum does not correspond (at least in the long-wavelength region) to that of the blackbody extrapolation, and therefore represents a separate emission component. Thus, the allowed N_H-corrected blackbody curves have to be below the *IUE* spectrum, constraining the blackbody temperature to the range 20–22 eV. The corresponding bolometric luminosity of the blackbody is obtained to be 2–5$\times 10^{32}$ erg s^{-1}/$< \cos\theta >$ for a distance of 100 pc. We note that using a white dwarf atmosphere model will predominantly reduce $L_{\rm BB}$ but result in a rather similar effective temperature.

4. Discussion

4.1. Possible accretion geometry

As shown in Sect. 3.2, the *ASCA* folded light curve shows little evidence of orbital modulation, while the low energy *ROSAT* light curves show a deep X-ray intensity modulation with an amplitude of 100%. This probably implies that the accretion pole moves around in the hemisphere of the white dwarf which is visible from the observer, and the X-ray modulation is caused by photoelectric absorption in the accretion column, as is also the case for the recently discovered new polar AX J2315−592 (Misaki et al. 1996, Thomas and Reinsch 1996).

From the *ROSAT* and *ASCA* light curves, we can estimate the hydrogen column density of the accretion column passing over the line of sight. Assuming the absorption by the column can be represented by a single hydrogen column density and the absorbing matter is cold, the PSPC response function predicts $N_{\rm H} > 8 \times 10^{20}$ cm^{-2} for the *ROSAT* counting rate in the band 0.1–0.5 keV to be reduced by 95%, if the blackbody parameters are the same as those out of the eclipse. On the other hand, for the *ASCA* counting rate (SIS+GIS) to be reduced less than 20% in the band 0.5–10 keV, the SIS and the GIS responses require $N_{\rm H} < 2 \times 10^{21}$ cm^{-2}. Therefore, the hydrogen column density of the accretion column passing over the line of sight at the time of eclipse is $\sim 10^{21}$ cm^{-2} on condition that the absorber is cold and can be characterized by a single hydrogen column density. As noted in Greiner, Remillard, Motch (1998), however, a detailed analysis of the energy resolved light curve of *ROSAT* indicates that the absorption by the column can hardly be reconciled with a single hydrogen column density. It is possible that the pre-shock column is ionized in part or has a distribution in $N_{\rm H}$ in the range $\lesssim 10^{21}$ cm^{-2}.

4.2. Evidence of postshock cooling flow

As explained in § 1, the hard X-ray spectrum of mCVs can usually be modelled by thermal bremsstrahlung with a single tem-

perature in the range 10–40 keV (Ishida and Fujimoto 1995). Although theories of the postshock accretion flow predict that the postshock plasma is cooled via thermal bremsstrahlung (Aizu 1973) and also cyclotron radiation (Wu et al. 1994, Woelk and Beuermann 1996) evidence of this cooling has been difficult to find observationally, because a thick ($N_{\rm H} \sim 10^{23}$ cm^{-2}), partial-covering absorption caused by the accretion column prevents us from measuring the shape of the intrinsic spectrum.

The only exception is EX Hya in which the hard X-ray continuum emission can be represented by a two temperature R&S model ($kT = 0.8$ keV and 8 keV) at first order approximation, and the ionization temperatures of heavy elements distribute in the range 0.9–8 keV (Ishida, Mukai and Osborne 1994). Fujimoto and Ishida (1997) showed that the distribution of the ionization temperatures is consistent with the postshock cooling flow predicted by Aizu (1973), and successfully determined the shock temperature and the mass of the white dwarf. The X-ray spectrum of RX J1802.1+1804 also requires two temperature R&S components, and is similar to that of EX Hya. We believe that *ASCA* observed the postshock cooling flow in RX J1802.1+1804.

This finding probably indicates that the temperature distribution due to the postshock cooling is a common feature among mCVs, and one always finds this as long as the low energy absorption is weak enough ($\leq 10^{21}$ cm^{-2}) as in EX Hya and RX J1802.1+1804.

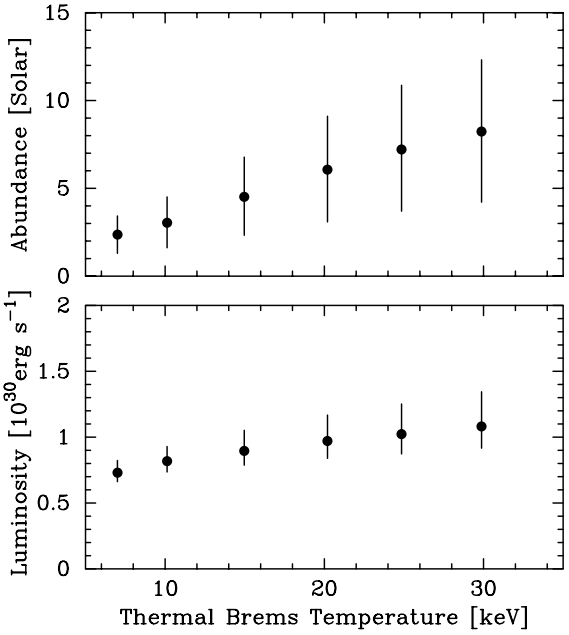

Fig. 8. The iron abundance of the plasma (upper panel) and the bolometric luminosity (lower panel) of the hard X-ray emission. For the luminosity, the distance to the source is assumed to be 100 pc.

4.3. Abundance

As displayed in Sect. 3, the hard part of the X-ray spectrum of RX J1802.1+1804 has a strong iron $K\alpha$ emission line with an equivalent width of $\sim$ 4 keV. The line originates from the hot plasma, and also, probably from the white dwarf surface via fluorescence (Hellier, Mukai and Osborne 1998). However, these two components cannot be resolved because of statistical limitations. In obtaining the elemental abundance of the plasma, we have to mix these two components so that the abundances they give are consistent.

As shown in Table 1, the temperature of the hard excess component is uncertain, with a lower limit of $\sim$ 7 keV. Therefore, we have fixed the temperature of the plasma at several trial values between 7 and 30 keV, and have made the following analysis. First, we have adopted thermal bremsstrahlung as the continuum spectrum. Then we have added three Gaussian lines which represent the fluorescent component at $\sim$ 6.4 keV, and He-like and hydrogenic components at 6.68 keV and 6.97 keV, respectively, and have performed the spectral fitting in the band 4–10 keV. In doing this, we have assumed that all the lines are narrow. Also the line central energies of the plasma components are fixed at 6.68 keV and 6.97 keV. The intensities of all the lines are constrained so that they give the same abundance at each fixed temperature. As mentioned in Sect. 3.3, the equivalent width of the fluorescent component should be 140 eV, almost irrespective of the plasma temperature, if the white dwarf surface has Solar composition. On the other hand, the equivalent widths of the plasma components can be obtained from the atomic data table in Raymond and Smith (1977) or Mewe et al. (1985) as a function of the plasma temperature in the case of Solar composition plasma. Therefore, the free parameters of the lines are only two — the central energy and the normalization of the fluorescent $K\alpha$ line. The fitting result thus obtained is shown in Fig. 8.

The resulting abundance is larger for higher trial temperature. This is a result of the fact that $K-$shell electrons are increasingly stripped off for higher temperatures, and hence a higher iron abundance is necessary to account for the observed equivalent width. The smallest abundance is obtained to be $2.4\pm1.1\odot$ at a temperature of 7 keV, which implies the lower limit of the abundance to be $1.3\odot$. Note, however, that this is a very conservative lower limit, and the abundance based on the iron $K\alpha$ emission line is probably several times as large as that of Solar composition. This is in contrast to the abundances of CVs which have recently been measured to be sub-Solar, such as $0.63\pm0.08\odot$ for EX Hya (Fujimoto and Ishida 1997), $0.4^{+0.2}_{-0.1}\odot$ for AM Her (Ishida et al. 1997), and $\sim 0.4\odot$ for SS Cyg (Done and Osborne 1997). A hint for a larger abundance than Solar is obtained only for AX J2315$-$592 (Misaki et al. 1996).

4.4. Luminosity of the hard X-ray component and the soft excess

Since we have obtained the abundance in the previous section, we have next calculated the bolometric luminosity of the hard X-ray component. To do this, we have adopted the volume emissivity formulas of the optically thin plasma approximated by

McCray (1987), but modified to take into account the abundance effects.

$$\Lambda(T, Z/Z_\odot) = 1.0 \times 10^{-22} \left(\frac{Z}{Z_\odot}\right) T_6^{-0.7} + 2.3 \times 10^{-24} T_6^{0.5} \quad [\mathrm{erg\ cm^3\ s^{-1}}],$$

where T_6 is the plasma temperature in 10^6 K. The first term on the right hand side is the volume emissivity for the line emission which is proportional to the abundance. The second term represents that of the free-free emission. Note that the first term is greater than the second term in the range $T < 2$ keV. The bolometric luminosity of the hard component $L_{\rm H}$ is obtained by $\Lambda \cdot EM$, where EM is the emission measure obtained from the spectral fitting for the 0.8 keV component and the hard excess component separately by assuming a distance to the source. The luminosity thus calculated for the trial temperatures is plotted in the lower panel of Fig. 8 showing a rather flat dependence with temperature in the 7–30 keV range: $L_{\rm H} = 0.6 - 1.4 \times 10^{30}$ erg s^{-1}. Note that we have not corrected for reflection from the white dwarf surface. One can do this by dividing the above value by $1 + a_X$ where a_X is the hard X-ray albedo.

In Sect. 3.4, we have obtained the lower limit of the bolometric luminosity of the blackbody component L_{BB} to be 2×10^{32} erg s^{-1} from *ROSAT* and *ASCA* simultaneous spectral fitting. This means $L_{\rm S}/L_{\rm H} > 140/ < \cos\theta >$. If we also take *IUE* data into account (Sect. 3.5), L_{BB} is constrained in the range $2 - 5 \times 10^{32}$ erg s^{-1}, and hence $L_{\rm S}/L_{\rm H} = (140 - 830)/ < \cos\theta >$ is obtained. Note that white dwarf atmosphere models could possibly reduce the luminosity of the soft component, and thus also $L_{\rm S}/L_{\rm H}$.

4.5. Note on determining parameters of the blackbody spectrum

In Sect. 3.4, we have derived the temperature of the soft blackbody component to be 15^{+7}_{-5} eV. The best fit value is outside the 'usual' range derived by Szkody et al. (1995), namely 20–45 eV. In estimating the blackbody temperature, Szkody et al. (1995) assumed a thermal bremsstrahlung component with a temperature of 10 keV for the hard X-ray component. However, based on our *ASCA* data we have found a spectral component which can be represented by a R&S spectrum with $kT \sim 0.8$ keV. The R&S component with such low temperature has a forest of iron emission lines in the 0.8–1 keV band caused by the iron L-shell transitions (Raymond and Smith 1977). Hence, a significant amount of the flux in the 0.8–2 keV band is attributed to the low temperature R&S component in our modelling. Note that this cannot happen if we assume a thermal bremsstrahlung component with a temperature of 10 keV. As a result, the blackbody temperature becomes lower than the estimates in Szkody et al. (1995).

In analyzing *ROSAT* data, one usually assumes the temperature of the hard X-ray component to be around 20 keV (Ramsay et al. 1994, for example). As shown here, however, this may cause a huge systematic error in evaluating the luminosity and the temperature of the soft blackbody component.

5. Conclusion

We presented X-ray data of RX J1802.1+1804 obtained by *ASCA*. From the *ASCA* light curves we find only marginal evidence for orbital intensity modulation which is seen in the *ROSAT* light curve below 0.5 keV characterized by the sharp and deep minima. From this energy dependence, we conclude that the intensity modulation is caused mostly by photoelectric absorption in the pre-shock accretion column, and the accreting pole moves around on the hemisphere visible from the observer, consistent with the conclusions from Greiner, Remillard & Motch (1998). It is possible that the line of sight absorber is partly ionized or has a distribution in N_H in the range $\lesssim 10^{21}$ cm^{-2}.

The X-ray spectrum can be represented by a two temperature optically thin thermal plasma emission model with temperatures of ~ 1 keV and > 7 keV. In analogy with EX Hya, we deduce that *ASCA* observed the cooling of the postshock plasma, as indicated by the theory of the postshock accretion flow. A remarkable feature of the X-ray spectrum of RX J1802.1+1804 is the strong iron $K\alpha$ emission line whose equivalent width is ~ 4 keV. To account for this, an iron abundance greater than Solar by at least 1.3 times is required. From the combined analysis of the *ROSAT* PSPC and *IUE* spectra, the ratio of the bolometric luminosity of the soft component to the hard is revealed to be greater than 140.

Acknowledgements. We are grateful for Dr. C.R. Shrader for supplying us with his *IUE* spectra. MI greatly appreciates financial support from JSPS along the Japan-Germany collaboration programme. JG is supported by the Deutsche Agentur für Raumfahrtangelegenheiten (DARA) GmbH under contract numbers FKZ 50 OR 9201 and 50 QQ 9602 3. RR acknowledges partial support from NASA grant NAG5–1784.

References

Aizu K., 1973, Prog. Theoret. Phys. 49, 1184
Arnaud K.A., 1996, Astronomical Data Analysis Software and Systems V, eds. Jacoby G. and Barnes J., ASP Conf. Ser. 101, p. 17
Beardmore A.P., Done C., Osborne J.P. and Ishida M., 1995, MNRAS 272, 749
Beuermann K. and Burwitz V., 1995, in Cape Workshop on Magnetic Cataclysmic Variables, eds. D. A. H. Buckley and B. Warner (ASP; San Francisco), p. 99
Burke B.E. et al., 1994, IEEE Trans. Nucl. Sci. 41, 375
Cropper M., 1990, Sp.Sci.Rev. 54, 195
Done C., Mulchaey J.S., Mushotzky R.F. and Arnaud K.A., 1992, ApJ 395, 275
Done C., Osborne J. P. and Beardmore A. P. 1995, MNRAS 276, 483
Done C. and Osborne J. P., 1997, MNRAS 288, 649
Frank J., King A.R. and Lasota J.P., 1983, MNRAS 202, 183
Fujimoto R. and Ishida M., 1997, ApJ 474, 774
George I.M. and Fabian A.C., 1991, MNRAS 249, 352
Greiner J., Remillard R.A. and Motch C., 1998, A&A 336, 191
Greiner J., Remillard R.A. and Motch C., 1995, in Cataclysmic Variables, eds. A. Bianchini, M. Della Valle and M. Orio (Dordrecht: Holland), p. 161
Hellier C., Mukai K. and Osborne J. P. 1998, MNRAS 297, 526

Imamura J. and Durisen, 1983, ApJ 268, 291
Ishida M., Mukai K. and Osborne J. P. 1994, PASJ 46, L81
Ishida M. and Fujimoto R., 1995, in Cataclysmic Variables, eds. A. Bianchini, M. Della Valle and M. Orio (Dordrecht: Holland), p. 93
Ishida M., Matsuzaki K., Fujimoto R., Mukai K. and Osborne J.P., 1997, MNRAS 287, 651
Makishima K. et al., 1996, PASJ 48, 171
Misaki K., Terashima Y., Kamata Y., Ishida M., Kunieda H. and Tawara Y., 1996, ApJ 470, L53
McCray R.A., 1987, in Spectroscopy of Astrophysical Plasma, ed. A. Dalgarno and D. Layzer (Cambridge University Press: Cambridge), p. 260
Norton A. J. and Watson M. G., 1989, MNRAS 237, 853
Ohashi T. et al., 1996, PASJ 46, 157
Ramsay G., Mason K.O., Cropper M., Watson M.G. and Clayton K.L., 1994, MNRAS 270, 692
Raymond J.C., Smith B.W., 1977, ApJ Suppl 35, 419
Rothschild R., et al. 1981, ApJ 250, 723
Serlemitsos P.J. et al., 1995, PASJ 47, 105
Shrader C.R., Singh K.P. and Barrett P., 1997, ApJ 485, 1006
Singh J. and Swank J.H., 1993, MNRAS 262, 1000
Szkody P., Silber A., Hoard D.W., Fierce E., Singh K.P., Barrett P., Schlegel E. and Piirola V., 1995, ApJ 455, L43
Thomas H. -C. and Reinsch K., 1996, A&A 315, L1
Woelk U. and Beuermann K., 1996, A&A 306, 232
Wu K., Chanmugam G. and Shaviv G., 1994, ApJ 426, 664
Yamashita A. et al., 1997, IEEE Trans. Nucl. Sci. 44, 847